AWARD NUMBER: W81XWH-17-1-0468

TITLE: Evaluation of Lipid Poor Renal Masses with Magnetic Resonance Spectroscopy in Tuberous Sclerosis Complex

PRINCIPAL INVESTIGATOR: Adam S. Feldman, M.D., M.P.H.

CONTRACTING ORGANIZATION: Massachusetts General Hospital, Boston, MA

REPORT DATE: December 2021

TYPE OF REPORT: Final

PREPARED FOR: U.S. Army Medical Research and Development Command
Fort Detrick, Maryland 21702-5012

REPORT DOCUMENTATION PAGE

Form Approved
OMB No. 0704-0188

1. REPORT DATE	2. REPORT TYPE	3. DATES COVERED
December 2021	Final	01Sep2017-31Aug2021

4. TITLE AND SUBTITLE

Evaluation of Lipid Poor Renal Masses with Magnetic Resonance Spectroscopy in Tuberous Sclerosis Complex

5a. CONTRACT NUMBER
W81XWH-17-1-0468

5b. GRANT NUMBER
***

5c. PROGRAM ELEMENT NUMBER

6. AUTHOR(S)

Adam S. Feldman, M.D., M.P.H.

5d. PROJECT NUMBER

5e. TASK NUMBER

5f. WORK UNIT NUMBER

7. PERFORMING ORGANIZATION NAME(S) AND ADDRESS(ES)

Massachusetts General Hospital
55 Fruit Street
Boston, Massachusetts 02114-2554

8. PERFORMING ORGANIZATION REPORT NUMBER

9. SPONSORING / MONITORING AGENCY NAME(S) AND ADDRESS(ES)

U.S. Army Medical Research and Development Command
Fort Detrick, Maryland 21702-5012

10. SPONSOR/MONITOR'S ACRONYM(S)

11. SPONSOR/MONITOR'S REPORT NUMBER(S)

12. DISTRIBUTION / AVAILABILITY STATEMENT

Approved for Public Release; Distribution Unlimited

13. SUPPLEMENTARY NOTES

14. ABSTRACT

The Research Project supported by this DOD Award investigates the potential of *in vivo* and *ex vivo* MRS in characterizing the metabolomic spectra of TSC-associated renal masses. Our goal is to gain an understanding of metabolomic markers in lipid poor renal masses which may be used in non-invasive imaging, as tissue based biomarkers, or as potential targets for future therapeutic development. To optimize our *in vivo* image acquisition protocol, we first scanned healthy volunteers. Our overall enrollment specifically of TSC patients with lipid poor renal masses had been lower than expected. In order to meet our goal of gaining more metabolomic data on renal masses, we expanded our subjects to include TSC patients with lipid rich masses, non-TSC patients with lipid poor and lipid rich renal masses. Our analysis cohort was also expanded with the utilization of our MGH Genitourinary Oncology Tumor Bank, including AML and other renal tumor tissue. Our *ex vivo* work from the tumor bank was presented virtually at the 2020 American Urological Association national meeting and was awarded Best Poster. The manuscript is currently in final editing for submission. In addition, we are analyzing our *in vivo* data and plan to prepare an additional manuscript. The findings from this study will help the TSC community gain an understanding of the metabolomics of AML and other renal tumors.

15. SUBJECT TERMS

Kidney Cancer; Metabolomics; Tuberous Sclerosis Complex

16. SECURITY CLASSIFICATION OF:			17. LIMITATION OF ABSTRACT	18. NUMBER OF PAGES	19a. NAME OF RESPONSIBLE PERSON
a. REPORT	b. ABSTRACT	c. THIS PAGE			USAMRDC
Unclassified	Unclassified	Unclassified	Unclassified	47	19b. TELEPHONE NUMBER *(include area code)*

Table of Contents

Page

Introduction…… 4

Keywords…… 4

Accomplishments…… 4-22

Impact…… 22-23

Changes/Problems…… 23-24

Products …… 24-25

Participants & Other Collaborating Organizations…… 25-29

Special Reporting Requirements…… 29

Appendix…… 30-47

Introduction:

The Research Project supported by this DOD Award investigates the potential of *in vivo* and *ex vivo* Magnetic Resonance Spectroscopy (MRS) in characterizing the metabolomic spectra of Tuberous Sclerosis Complex (TSC)-associated lipid poor renal masses. We have hypothesized that MRS metabolomic profiling of lipid poor renal masses will provide clinical biomarkers to noninvasively differentiate benign from malignant tumors and can help predict the tumor grades and pathological stages defined by histopathology, thus improving decision making for patient care. This information is urgently needed in today's TSC clinic to help clinicians to assess the malignant potentials of specific tumors, improve prognostic accuracy, and select the most appropriate therapy for individual patients.

Keywords:

Tuberous Sclerosis Complex; Metabolomics; Kidney Cancer; Biomarker

Accomplishments:

- **What were the major goals of the project?**
  There are three defined major goals of the project to be accomplished over the course of a 24 month period, with a 12 month no-cost extension:

  Major Task 1: Administrative startup tasks; Subject recruitment (total n=80); *In vivo* MRI/MRS acquisition and interpretation, with correlation of MRS data with multiparametric MRI data; Histopathologic analysis of biopsy and surgical specimens; Correlation of *in vivo* MRS data with histopathology and clinical data.

  Major Task 2: *Ex vivo* MRS performance on biopsy and surgical specimens; Correlation of *ex vivo* MRS data with histopathology and clinical data; Assess consistency of *in vivo* and *ex vivo* MRS metabolomic signatures and correlate signatures with tumor tissue assessment for mutations of the cellular metabolic pathway and direct measurement of

tumor metabolite levels.

Major Task 3: Correlation of *ex vivo* and *in vivo* MRS data; GC-MS and qRT-PCR of surgical tissue specimens; Correlation of all MRS, histopathologic and clinical data with GC-MS and qRT-PCR data.

What was accomplished under these goals?

General update:

We were given local IRB approval for the research project in January 2018. Subject enrollment began in February 2018 with patients recruited from the Urology Clinic at Massachusetts General Hospital. Given that there has been limited data in performing *in vivo* MRS of the kidney, healthy volunteers were first consented to the project to undergo *in vivo* MRS and help develop the imaging protocol for ultimate subject scans.

Since the project start, 22 research subjects have been consented and underwent multiparametric MRI and MRS of the kidneys. Fourteen of the subjects have confirmed diagnoses of Tuberous Sclerosis Complex, while eight of the subjects have sporadic renal masses. Four have undergone clinically-indicated renal mass biopsy (RMB) with core biopsy specimens evaluated with *ex vivo* MRS immediately after RMB. Five subjects have had partial nephrectomies and had tissue evaluated with *ex vivo* MRS immediately after.

As noted in previous reports, given the slow rate of recruitment of patients with TSC, we elected to augment our study with *ex vivo* MRS analysis on 89 specimens from 55 subjects from our MGH GU Oncology Frozen Tumor Bank. One difficulty with recruitment has been that as a referral institution, many patients who we see have already had their appropriate renal mass imaging performed and therefore, an additional study cannot be justified in their clinical care. The specimens for *ex vivo* MRS from our tissue bank were collected from 55 unique patients who underwent radical or partial nephrectomy. Seven specimens were of angiomyolipoma, 13 papillary RCC, 21 clear cell RCC, 13 chromophobe RCC, 10 oncocytoma, and 25 benign tissue specimens adjacent to one of the previously mentioned. High-resolution magic angle spinning (1H HRMAS) ex vivo MRS spectra images were obtained. This work was been presented at the

2020 American Urological Association national meeting and was awarded Best Poster. Since our previous update a manuscript has been prepared and is in final editing stages for submission. The manuscript is attached to the report in the appendix.

Detailed info on prospective patient *in vivo* and *ex vivo* work:

Over the course of the study period, twenty-two patients underwent clinical MRI with additional in vivo MRS sequences. Fourteen patients were TSC patients and eight were patients with sporadic renal masses. The routine multi-parametric renal MRI includes multiecho gradient-echo, diffusion weighted images with 3 b values (0, 500 and 1000) and dynamic enhanced images with temporal resolution of 6 seconds. Two single voxels (Volume of interest (VOI = 2 x 2 x 2 cm3) are targeted over the area of interest for the *in vivo* MRS spectra. We ran prior axial and coronal imaging sequences with non-breath hold technique to use as references for the MRS sequences. Metabolic spectra of both the tumor(s) of interest and regions of benign parenchymal tissue were recorded and analyzed. We used a respiratory-gated Point Resolved Spectroscopy (PRESS) sequence with and without water suppression using TE/TR=135ms/1500ms and number of averages (NA) = 32 for the water-suppressed spectrum and NA = 4 for the water-unsuppressed sequence.

Over the course of the study period we obtained and analyzed the metabolomic spectra of the lesions of interest and healthy parenchymal tissue as previously reported in our quarterly and annual reports. In patients with multiple masses we obtained metabolic spectra from multiple lesions. Figure 1 demonstrates a representation of the *in vivo* metabolomic spectra. This is from a patient with TSC and multiple renal lesions, with the lesion of interest here being a lipid-poor renal mass which had previously been biopsied and found to be a renal oncocytoma, a benign lesion. Metabolomic spectra were obtained from the lesion of interest as well as the normal renal parenchyma and demonstrate subtle differences in peaks.

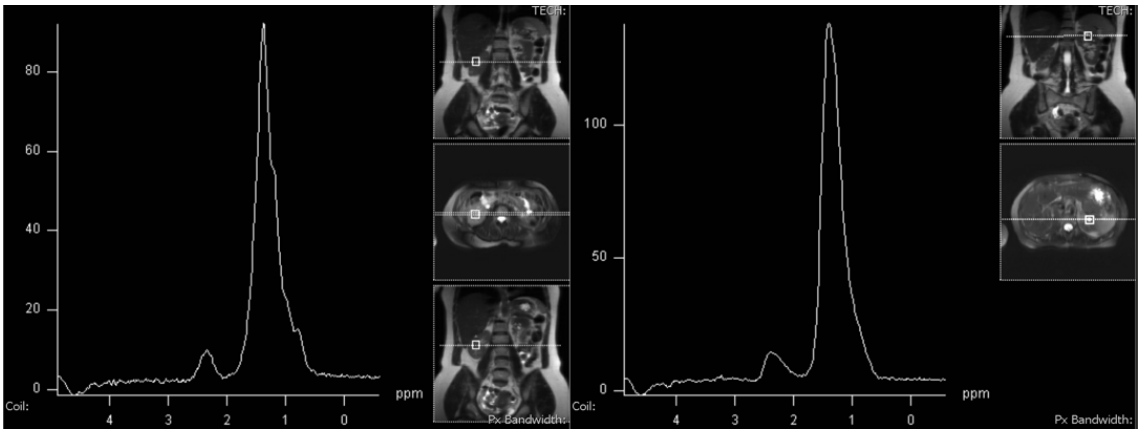

Figure 1: Example of in vivo MRS spectra from a single patient with history of TSC. The image on the left obtained with targeting normal parenchymal renal tissue. The image on the right obtained with targeting the previous biopsy-proven oncocytoma.

Figure 2 demonstrates a representative metabolomic spectra from a patient with a large AML requiring embolization. In comparison of the spectra from the normal parenchyma and the renal lesion, there are clear spectral differences with greater metabolic variability in the AML. In addition, the comparison of the renal lesion spectra between Figures 1 and 2 also demonstrate spectral differences between the oncocytoma and AML.

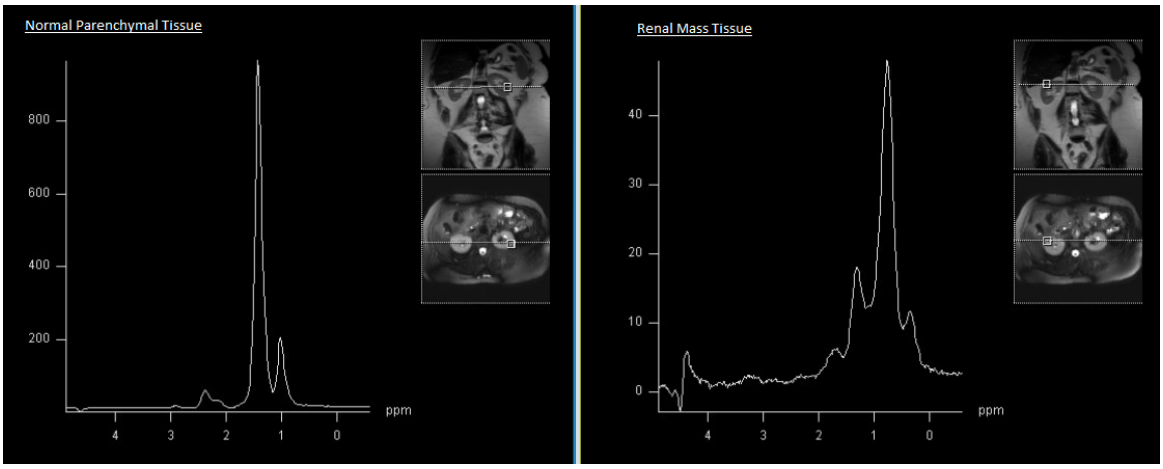

Figure 2: Example of in vivo MRS spectra from a patient without a history of TSC. The image on the left obtained with targeting contralateral normal kidney tissue. The image on the right obtained with targeting of large angiomyolipoma requiring embolization.

Figure 3 shows a representative image from a TSC patient with bilateral AMLs and RCCs. Two separate lesions were imaged with *in vivo* MRS and then ultimately underwent percutaneous renal mass biopsy. The right lesion was biopsied and found to be a lipid poor AML. The left lesion was biopsied and then underwent partial nephrectomy demonstrating an oncocytic RCC.

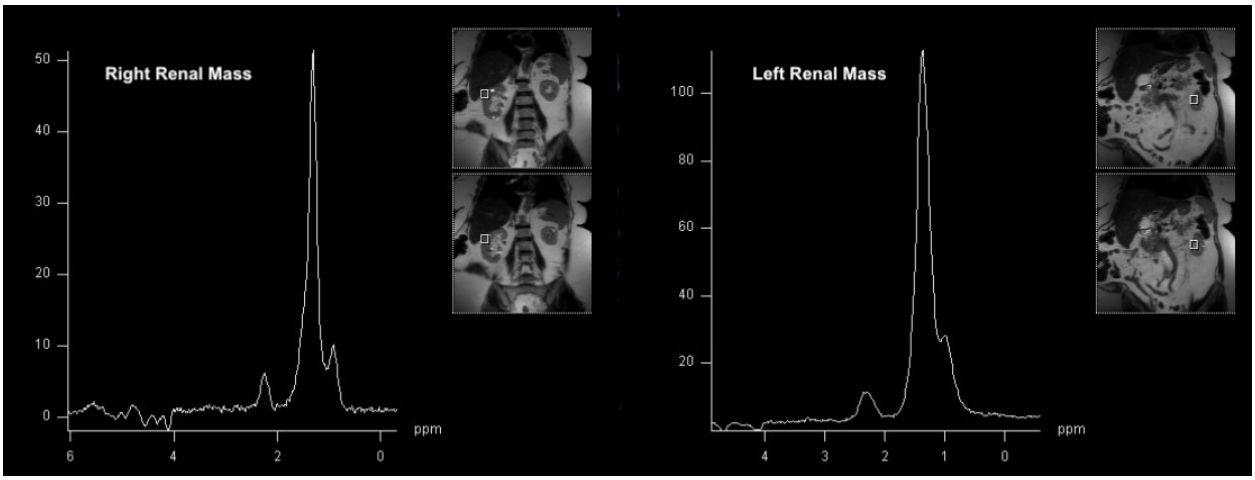

Figure 3: Example of in vivo MRS spectra from a single patient with history of TSC and bilateral renal AMLs and RCCs. The image on the left obtained with targeting the right renal mass. The image on the right obtained with targeting the left renal mass.

In addition to the metabolomic spectra from TSC patients as shown above, non-TSC patients with sporadic renal masses were also included. Figure 4 represents one of the examples of the metabolomic spectra from a non-TSC patient with a sporadic renal mass.

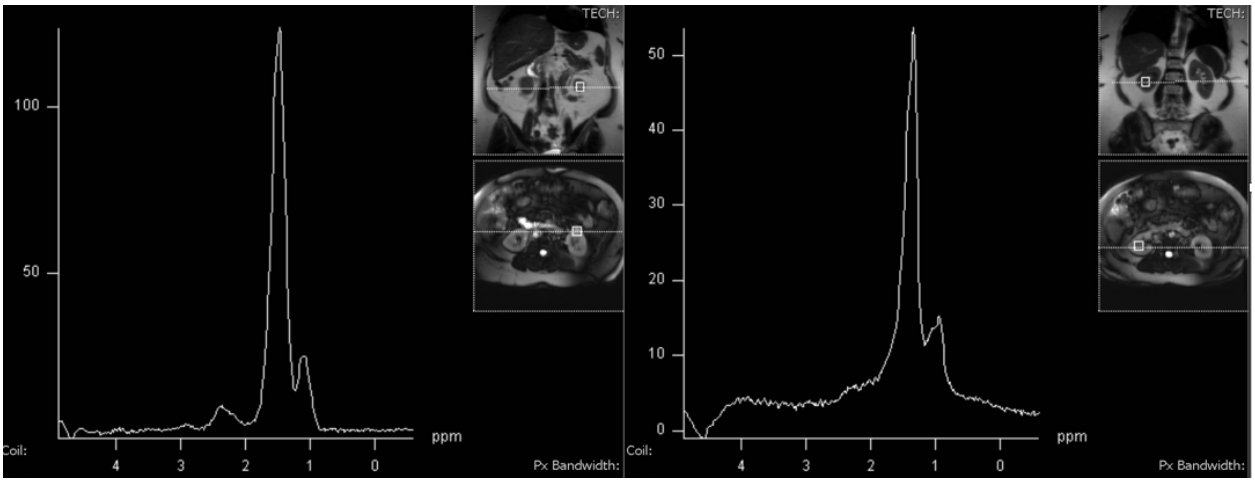

Figure 4: Example of in vivo MRS spectra from a patient without a history of TSC. The image on the right obtained with targeting of normal renal parenchymal tissue. Image on the left obtained with targeting contralateral, left renal lesion, RCC favored by radiographic review.

These representative images of the *in vivo* metabolomic spectra demonstrate the subtle heterogeneity of spectra between normal parenchyma and renal masses of different etiology. As we have analyzed our *in vivo* data between mass types, unfortunately we have not seen clear differences between AML and renal epithelial neoplasms (RCC and oncocytoma). With improvements in analytics, we are planning to use a more AI-based analysis of the raw data to assess for any potential overall signatures.

Of patients who underwent *in vivo* MRS, a handful of the patients had biopsy or surgical tissue available for *ex vivo* MRS analysis. Immediately after RMB, core biopsy specimens were transported on ice to the A.A. Martinos Center for Biomedical Imaging at MGH for *ex vivo* MRS. For those who had surgery for excision of the renal mass, following resection, the specimens were taken to the Surgical Pathology lab as soon as possible to minimize changes in the metabolomic profile from devascularization. Following MRS, the specimens were transported to the MGH Pathology department for routine histopathologic processing. Similar to biopsy specimens, specimens were then transported on ice to the A.A. Martinos Center for Biomedical Imaging at MGH for *ex vivo* MRS. The metabolic spectra of all specimens were recorded and analyzed.

One patient who underwent renal mass biopsy had a history of TSC with numerous bilaterial lesions. Metabolic spectra one of the lesions of interest were obtained and demonstrated the various peaks along the metabolomic spectrum (Figure 5). Histopathology of this lesion demonstrated lipid poor AML. Among the peaks are those for known metabolites, including lactate, creatine, taurine and choline compounds. The role these play in the pathogenesis of AML is as of yet unclear.

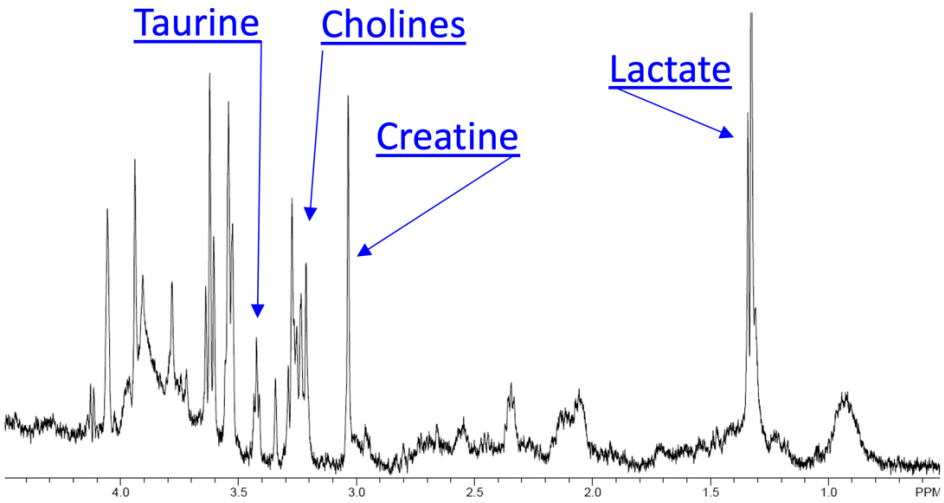

Figure 5: Example of high-resolution magic angle spinning (1H HRMAS) ex vivo MRS spectra image obtained with intact biopsy-core specimen from fat-poor angiomyolipoma kidney tissue from single patient

For one patient who underwent surgical resection of a renal mass, the histopathologic analysis of the surgical specimen was consistent with clear cell Renal Cell Carcinoma (ccRCC), stage T1a, grade 2, with no evidence of tumor necrosis or lymphovascular invasion. The example of this spectra is present in Figure 6 and shows multiple lipid peaks, as well as lower spectral changes in choline compounds.

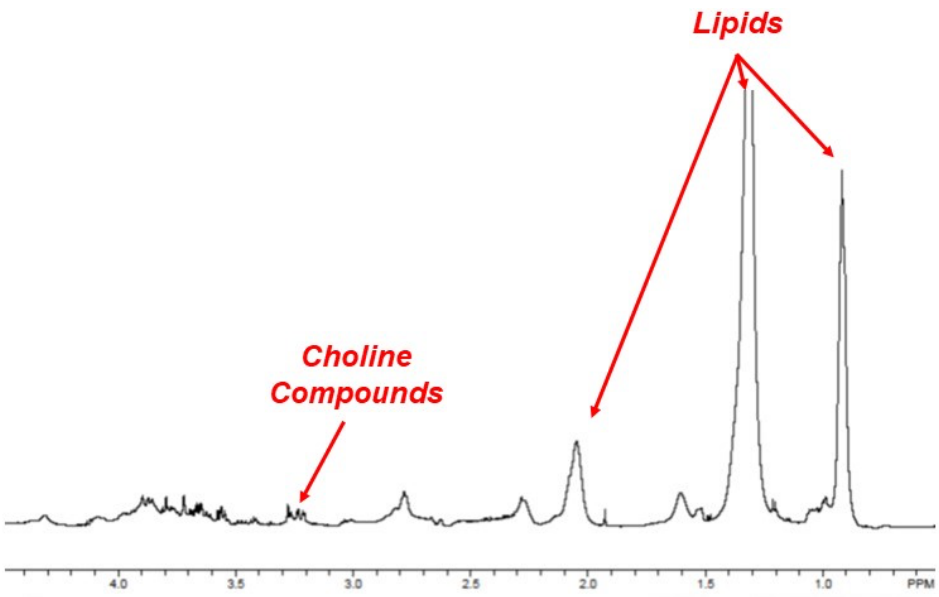

Figure 6: Example of high-resolution magic angle spinning (^{1}H HRMAS) *ex vivo* MRS spectra image obtained with intact partial nephrectomy specimen from renal cell carcinoma, clear cell type kidney tissue from single patient.

Additionally a sporadic renal mass patient, who underwent in vivo MRS with MRI from the prior reporting period, underwent partial nephrectomy of a left posterior midpole lesion. Histopathologic analysis confirmed Type 1 Papillary Renal Cell Carcinoma. On immunohistochemical stain, the tumor cells are positive for CK7, CD10 and focally positive for CD57 and negative for WT1 and BRAF, supporting the diagnosis. Metabolic spectra of the lesion of interest were obtained (Figure 7). These findings demonstrated the highest peaks for known metabolite locations including lactate, choline compounds, alanine and lipids.

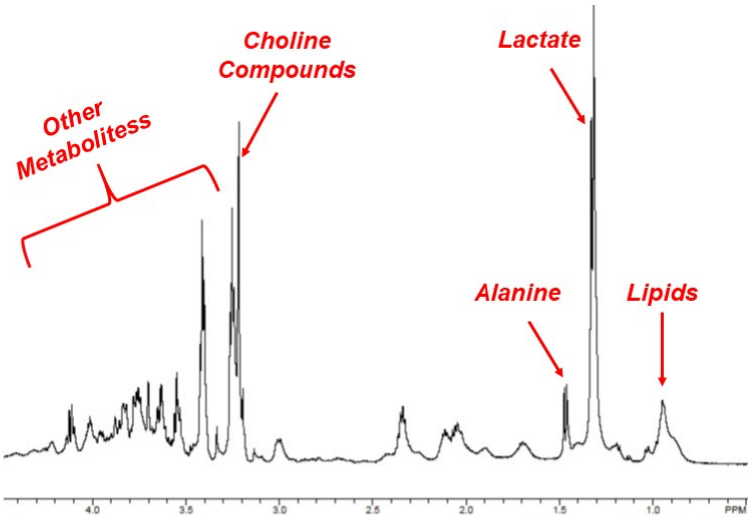

Figure 7: Example of high-resolution magic angle spinning (1H HRMAS) ex vivo MRS spectra image obtained from partial nephrectomy specimen of Papillary Type 1 RCC.

These metabolomic findings by MRS on fresh biopsy tissue and surgical specimens prompted our investigation of renal masses in fresh frozen tissue from our MGH GU Tumor Bank. This also became a necessary alternative plan for investigating MRS given our lower than anticipated accrual. For internal quality control (unpublished data), we have previously tested and compared the adequacy of *ex vivo* MRS analysis with fresh tissue vs. fresh frozen tissue. We have not identified any differences in the quality of metabolomic spectra, or differences in the reproducibility of results. Our investigation of renal mass tissue from the MGH GU Tumor Bank is discussed below.

Detailed info on *ex vivo* analysis of MGH GU Tumor Bank fresh frozen tissue:

In order to improve our subject size and meet our goals of *ex vivo* analysis, we have taken advantage of our previously collected and annotated MGH GU Oncology Frozen Tumor Bank. Our internal IRB for utilization of tissue bank specimens was approved on 2/27/2020. After approval we began our analysis of these specimens. This tumor bank includes fresh frozen tissue from renal masses, including benign renal neoplasms, angiomyolipoma and RCC.

We completed ex vivo MRS on 89 specimens stored in the tumor bank. These were collected from 55 unique patients who underwent radical or partial nephrectomy. Seven specimens were of angiomyolipoma, 13 papillary RCC, 21 clear cell RCC, 13 chromophobe rcc, 10 oncocytoma, and 25 benign tissue adjacent to one of the previously mentioned. High-resolution magic angle spinning (1H HRMAS) ex vivo MRS spectra images were obtained and example spectra are presented below (Figures 8-12).

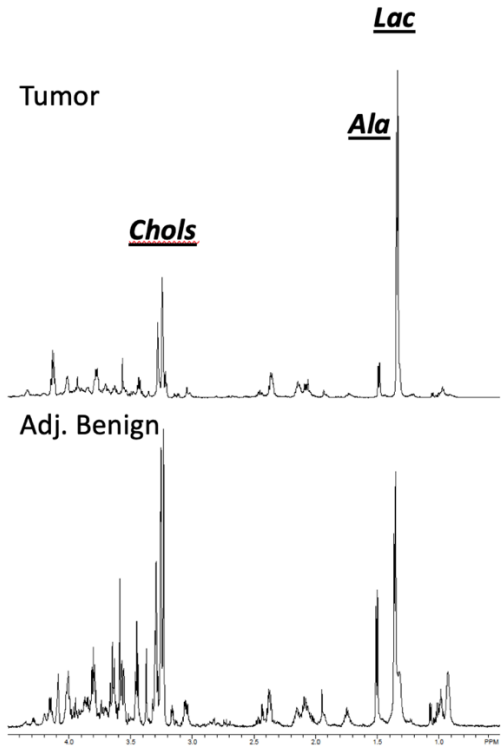

Figure 8: Example of high-resolution magic angle spinning (^{1}H HRMAS) *ex vivo* MRS spectra image obtained from fresh frozen tumor bank specimen of intact partial nephrectomy specimen from renal cell carcinoma, clear cell type kidney tissue and adjacent benign tissue from single patient.

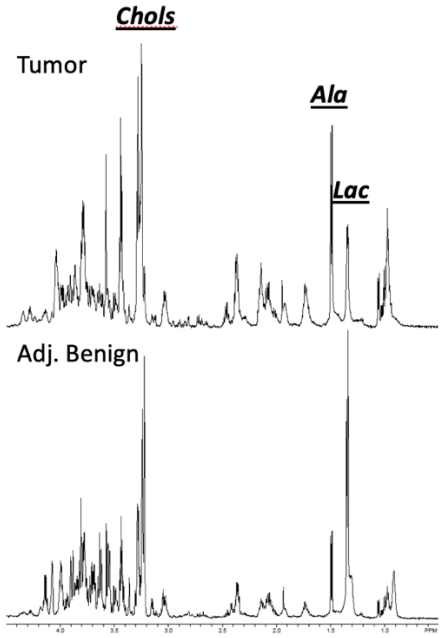

Figure 9: Example of high-resolution magic angle spinning (^{1}H HRMAS) *ex vivo* MRS spectra image obtained from fresh frozen tumor bank specimen of intact partial nephrectomy specimen from renal cell carcinoma, papillary type kidney tissue and adjacent benign tissue from single patient.

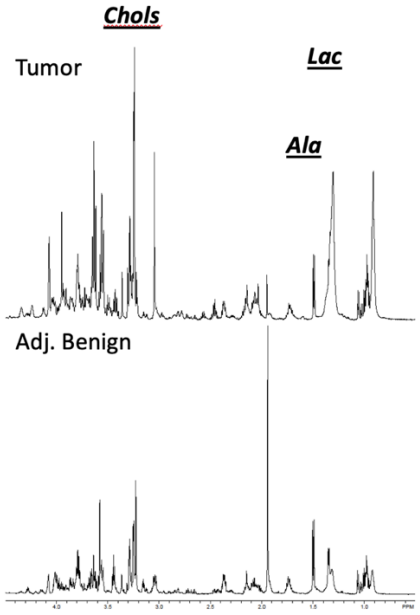

Figure 10: Example of high-resolution magic angle spinning (^{1}H HRMAS) *ex vivo* MRS spectra image obtained from fresh frozen tumor bank specimen of intact partial nephrectomy specimen from renal cell carcinoma, chromophobe type kidney tissue and adjacent benign tissue from single patient.

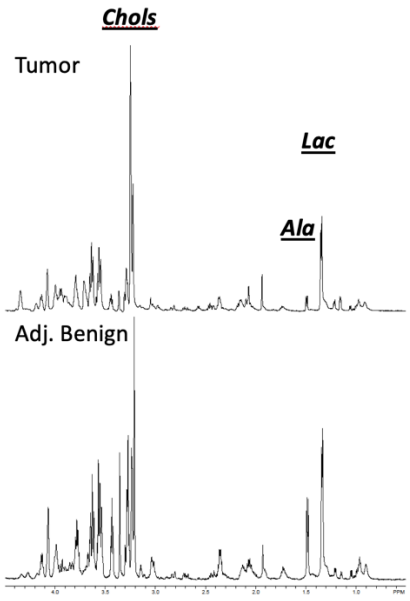

Figure 11: Example of high-resolution magic angle spinning (^{1}H HRMAS) *ex vivo* MRS spectra image obtained from fresh frozen tumor bank specimen of intact partial nephrectomy specimen from oncocytoma kidney tissue and adjacent tissue from single patient.

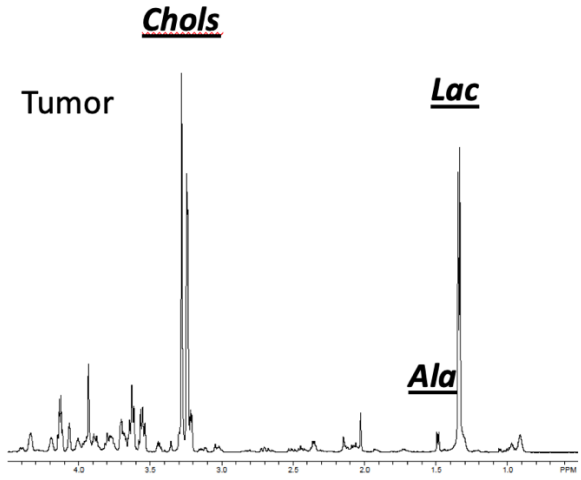

Figure 12: Example of high-resolution magic angle spinning (^{1}H HRMAS) *ex vivo* MRS spectra image obtained from fresh frozen tumor bank specimen of intact partial nephrectomy specimen from angiomyolipoma kidney tissue from single patient.

To further investigate the metabolomic profile of RCC, we initially compared our RCC specimens to adjacent benign renal parenchyma and this was outlined in our 2020 Annual

Report. To better compare RCC with other renal masses, we then compared the tumor metabolomic profiles from 38 patients with RCC (16 clear cell, 11 papillary, 11 chromophobe) and 17 patients with benign tumors. We also included the adjacent benign renal parenchyma in our analyses. Of the RCC specimens 13 had adjacent normal tissue specimens available. Of benign tumors, there were 10 oncocytomas and 7 AMLs, and there was adjacent normal tissue for 5 of these samples. Baseline characteristics are presented in Table 1.

Table 1. Baseline patient characteristics

	RCC (N=38)	**Benign tumors (N=17)**	**P-value**
Age (years) (mean ± SD)	55.3 ± 11.4	59.2 ± 12.2	0.2651
Sex (n, %)			0.012
Males	27 (71)	6 (35.3)	
Females	11 (29)	11 (64.7)	
Race (n, %)			0.260
White	97 (97.4)	16 (94.1)	
Black	0 (0)	0 (0)	
Hispanic	1 (2.6)	1 (5.9)	
Surgery			0.965
Radical nephrectomy	22 (59.5)	10 (58.8)	
Partial nephrectomy	15 (40.4)	7 (41.2)	
Missing	1 (2.6)	0 (0)	
Median tumor size (cm, IQR)	4.35 (3.2, 6.5)	4.9 (3.3, 8)	0.5496
Tumor Stage (n, %)			N/A
T1	26 (70.3)	-	
T2	2 (5.4)	-	
T3	9 (23.7)	-	
T4	0 (9)	-	
Missing	1 (2.6)	-	

Surgical tissue samples utilized from our frozen tissue bank were initially obtained from radical nephrectomy or partial nephrectomy. Specimens were frozen and then stored at -80ºC for at least 24 hours until the time of analysis. Tissue HRMAS-MRS was performed on a Bruker AVANCE spectrometer operating at 600 MHz. Three different spectra were recorded at 4ºC: one without water suppression, one with water suppression and long *T2* filters, and one with water suppression and short *T2* filters.

A MatLab-based curve fitting program developed by our laboratory was used to process the spectra to produce relative intensities for each analyzed spectral region of interest. There were 59 spectral

regions of interest, and comparisons of the metabolomic profiles were performed using JMP Pro 14 (*Cary, NC*). Comparisons were made between RCC and benign tissue adjacent to the malignant tumor, as well as between RCC and benign tumors. False discovery rates (FDR) were used from the response screening to account for multiple testing. Regions of interest (ROI) with FDR <0.05 were reported as potential predictors of RCC rather than benign tumor or benign tissue adjacent to malignant tumor. Based on these results, the Wilcoxon rank sum test was used to compare the median MRS relative intensities for those metabolites that may differentiate between RCC and either benign tumor or benign tissue adjacent to malignant tumor. Logistic regression was used to determine odds ratios for risk of malignancy based on the abundance of each metabolite.

Comparisons of median MRS relative intensities for RCC (n=38) versus tissue adjacent to the malignant tumor (n=13) are presented in Table 2. Only statistically significant spectral regions based on FDR screening are reported. There were 60 ROIs tested, and 16 were found to be statistically significant. Those denoted as TBD (to be determined) are undergoing further study to definitively identify and associate specific metabolites to the corresponding spectral regions.

Table 2. Comparison of median relative intensities (IQR) of RCC vs. tissue adjacent to malignant tumor

ROI (ppm)	RCC (N=38)	Tissue adjacent to malignant tumor (N=13)	Wilcoxon rank sum P-value	FDR P-value
4.07-4.05 (Myo-Inositol)	0.80 (0.50, 1.30)	1.85 (1.44, 2.24)	0.0025	0.026
4.02-4.00 (TBD)	1.21 (0.69, 2.06)	0.50 (0.22, 0.85)	0.0069	0.033
3.99-3.96 (Histidine, Phenylalanine, Phosphocholine, Serine)	1.26 (0.87, 1.89)	2.56 (1.46, 3.37)	0.0089	0.011
3.95-3.94 (Serine, Phosphocreatine)	0.77 (0.33, 1.19)	0.30 (0.002, 0.46)	0.0006	0.002
3.93-3.91 (Creatine, Glycerophosphocholine)	1.28 (0.91, 1.60)	0.69 (0.30, 1.31)	0.0069	0.011
3.61-3.59 (Myo-Inositol, Glycerophosphocholine,	0.96 (0.65, 1.20)	1.68 (1.49, 1.93)	0.0005	0.004
3.55-3.52 (Glycine)	1.92 (1.34, 3.10)	4.03 (2.90, 4.32)	0.0019	0.022
3.36-3.34 (Scylla-Inositol)	0.55 (0.35, 0.77)	1.34 (0.91, 1.53)	0.0019	0.004
3.24-3.23 (Myo-Inositol, Taurine)	5.86 (3.97, 9.42)	4.32 (2.61, 5.20)	0.0260	0.028
3.22-3.21 (Phosphocholine, Glycerophosphocholine, Histidine)	0.69 (0.24, 2.06)	4.23 (3.46, 5.42)	<0.001	1.570×10^{-4}
3.15-3.13 (Spermine, Histidine, Phenylalanine)	0.21 (0.11, 0.35)	0.83 (0.49, 0.99)	<0.001	1.025×10^{-4}

2.84-2.82 (TBD)	0.28 (0.18, 0.45)	0.18 (0.12, 0.22)	0.0020	$4.792x10^{-4}$
2.45-2.42 (Glutamine)	0.51 (0.31, 0.73)	0.32 (0.24, 0.38)	0.0095	0.008
2.15-2.11 (Glu,Gln,glutathione)	1.95 (1.47, 2.46)	1.45 (1.26, 1.91)	0.0360	0.016
1.93-1.92 (Acetoacetate)	0.31 (0.19, 0.67)	0.77 (0.58, 1.63)	0.0008	0.034
1.35-1.33 (Lactate)	8.73 (5.53, 13.2)	5.24 (3.08, 8.07)	0.0146	0.011

Table 3 summarizes the ROIs that were found to differ in median MRS relative intensity and the odds ratios for risk of malignancy based on relative abundance. Of particular note, there was a greater amount of serine and phosphocreatine (3.95-3.94 ppm) in RCC specimens, with an odds ratio of 29.24 [95% CI: 2.47, 345.94], p=0.007, as well as glutamine (2.45-2.42 ppm) (OR 121.56 [95% CI 2.17, 6825.42]). There are also a number of metabolites in other spectral regions that differed in quantity between RCC and the tissue adjacent to the malignant tumor, the exact identities of which have yet to be elucidated. The greatest odds ratio for risk of malignancy was observed for metabolites in the 2.84-2.82 spectral region (7161.72 [95% CI 6.30, 8.14x106], p=0.013).

Table 3. Odds ratios for risk of malignancy for metabolites identified as potential predictors of malignancy based on FDR P-value (reference group: tissue adjacent to malignant tumor)

Region of interest (ppm)	Odds ratios (OR, 95% CI)	P-value for OR
4.07-4.05 (Myo-Inositol, G6P, Tryptophan)	0.38 (0.18, 0.82)	0.013
4.02-4.00 (TBD)	3.13 (1.10, 8.85)	0.032
3.99-3.96 (Histidine, Phenylalanine, Phosphocholine, Serine)	0.34 (0.16, 0.71)	0.004
3.95-3.94 (Serine, Phosphocreatine)	29.24 (2.47, 345.94)	0.007
3.93-3.91 (Creatine, Glycerophosphocholine)	8.17 (1.77, 37.78)	0.007
3.61-3.59 (Myo-Inositol, Glycerophosphocholine)	0.13 (0.03, 0.490)	0.003
3.55-3.52 (Glycine)	0.59 (0.39, 0.90)	0.014
3.36-3.34 (Scylla-Inositol)	0.08 (0.02, 0.42)	0.003
3.24-3.23 (Myo-Inositol, Taurine)	1.35 (1.04, 1.76)	0.027
3.22-3.21 (Phosphocholine, Glycerophosphocholine, Histidine)	0.41 (0.25, 0.67)	<0.001
3.15-3.13 (Spermine, Histidine, Phenylalanine)	$3.72x10^{-5}$ ($7.42x10^{-8}$, $1.87x10^{-2}$)	0.001
2.84-2.82 (TBD)	7161.72 (6.30, $8.14x10^{6}$)	0.013
2.45-2.42 (Glutamine)	121.56 (2.17, 6825.42)	0.02
2.15-2.11 (Glu,Gln,GSH)	3.96 (1.18, 13.28)	0.026
1.93-1.92 (Acetoacetate)	0.38 (1.13, 1.09)	0.072
1.35-1.33 (Lactate)	1.22 (1.03, 1.45)	0.023

Comparisons of median MRS relative intensities for statistically significant spectral regions based on FDR screening for RCC (n=38) and benign tumor (n=17) are presented in Table 4. There were 25 ROIs found to be candidates for predictors of RCC, with FDR<0.05. Table 5 summarizes the ROIs that were found to differ in median MRS relative intensity and the odds ratios for risk of malignancy based on relative abundance. ROIs associated with significantly elevated risk of malignancy include: 4.09-4.08 (OR 6.67x107, 95% CI 1.47, 3.01x1015), 3.9-3.89 (creatine, glycerophosphocholine; OR 155.04, 95% CI 8.49, 2.83x103), 3.5-3.49 (OR 5.15x103, 95% CI 25.82, 1.03x106), 3.15-3.13 (spermine, histidine, phenylalanine; OR 339.30, 95% CI 2.44, 4.72x104), 3.12-3.09 (polyamines; OR 4.81x103, 95% CI 9.53, 2.43x106), 2.38-2.37 (OR 4.21x104, 95% CI 20, 8.87x107), 1.91-1.89 (OR 59.05, 95% CI 3.63, 961.34), and 1.75-1.74 (OR 2.87x103, 95% CI 5.33, 1.55x106) ppm spectral regions.

Table 4. Comparison of median relative intensities (IQR) of RCC vs. benign tumor

ROI (ppm)	RCC (N=38)	Benign tumor (N=17)	Wilcoxon rank sum P-value	FDR P-value
4.09-4.08 (TBD)	0.04 (0.0007, 0.1226)	0.0017 (0.0002, 0.0039)	0.0067	0.010
4.07-4.05 (Myo-Inositol, G6P, Tryptophan))	0.80 (0.50, 1.30)	1.78 (1.19, 2.65)	0.0097	0.016
4.02-4.00 (TBD)	1.21 (0.69, 2.06)	0.25 (0.13, 0.57)	0.0002	3.352×10^{-4}
3.9-3.89 (Cr, GPC)	0.90 (0.58, 1.13)	0.42 (0.10. 0.68)	<0.001	6.573×10^{-5}
3.86-3.85 (TBD)	0.81 (0.43, 1.14)	0.16 (0.008, 0.39)	<0.001	6.573×10^{-5}
3.84-3.81 (Glc)	1.30 (0.96, 1.70)	0.59 (0.03, 0.97)	0.0002	3.352×10^{-4}
3.61-3.59 (Myo-Inositol, Glycerophosphocholine,	0.96 (0.65, 1.29)	1.85 (1.58, 2.23)	0.0025	0.004
3.57-3.56 (Gly)	1.69 (1.29, 2.19)	1.14 (0.16, 1.49)	0.0040	0.020
3.55-3.52 (Glycine)	1.92 (1.34, 3.10)	3.62 (2.42, 6.12)	0.0197	0.020
3.5-3.49 (TBD)	0.31 (0.17, 0.59)	0.008 (0.0003, 0.12)	<0.001	6.573×10^{-5}
3.48-3.46 (TBD)	0.56 (0.33, 0.87)	0.05 (0.006, 0.35)	0.0028	0.011
3.45-3.43 (TBD)	1.20 (0.77, 2.32)	0.60 (0.32, 0.87)	0.0013	0.004
3.42-3.39 (Glc, Taurine)	1.37 (0.89, 2.81)	0.59 (0.25, 1.28)	0.0032	0.010
3.15-3.13 (Spermine, Histidine, Phenylalanine)	0.21 (0.11, 0.35)	0.13 (0.002, 0.21)	0.0133	0.040
3.12-3.09 (polyamines)	0.22 (0.13, 0.32)	0.08 (0.009, 0.16)	0.0015	0.020
2.38-2.37 (TBD)	0.26 (0.18, 0.35)	0.16 (0.08, 0.24)	0.003	0.008
2.36-2.31 (Glutamate)	1.91 (1.32, 2.76)	1.47 (0.12, 1.84)	0.0197	0.002
2.15-2.11 (Glu,Gln, glutathione)	1.95 (1.47, 2.46)	1.27 (0.68, 1.69)	0.002	0.020
1.91-1.89 (TBD)	0.46 (0.24, 0.66)	0.19 (0.0003, 0.26)	0.001	0.002
1.75-1.74 (TBD)	0.21 (0.14, 0.35)	0.09 (0.06, 0.16)	0.004	0.004
1.73-1.63 (TBD)	1.35 (0.84, 1.90)	0.67 (0.41, 0.95)	0.0011	0.008
1.6-1.57 (TBD)	0.08 (0.0005, 0.19)	0.19 (0.002, 0.49)	0.0197	0.002
1.49-1.46 (Alanine)	2.03 (2.84, 1.52)	1.06 (0.46, 1.25)	<0.001	0.010
1.06-1.03 (Valine)	0.61 (0.28, 0.89)	0.28 (0.11, 0.39)	0.007	6.573×10^{-5}
1.00-0.94 (Valine, Lipids)	2.75 (1.89, 4.19)	1.47 (0.96, 2.48)	0.0108	0.010

Table 5. Odds ratios for risk of malignancy for metabolites identified as potential predictors of malignancy based on FDR P-value (reference group: benign tumor)

Region of interest (ppm)	Odds ratios (OR, 95% CI)	P-value for OR
4.09-4.08 (TBD)	$6.67x10^{7}$ (1.47, $3.01x10^{15}$)	0.045
4.07-4.05 (Myo-Inositol, G6P, Tryptophan))	0.45 (0.25, 0.82)	0.009
4.02-4.00 (TBD)	7.61 (2.04, 28.35)	0.002
3.9-3.89 (Cr, GPC)	155.04 (8.49, $2.83x10^{3}$)	0.001
3.86-3.85 (TBD)	61.72 (5.75, 662)	0.001
3.84-3.81 (Glc)	10.5 (2.68, 41.22)	0.001
3.61-3.59 (Myo-Inositol, Glycerophosphocholine,	0.24 (0.09, 0.62)	0.003
3.57-3.56 (Gly)	2.98 (1.21, 7.35)	0.018
3.55-3.52 (Glycine)	0.68 (0.50, 0.92)	0.012
3.5-3.49 (TBD)	$5.15x10^{3}$ (25.82, $1.03x10^{6}$)	0.002
3.48-3.46 (TBD)	9.90 (1.51, 64.89)	0.017
3.45-3.43 (TBD)	3.84 (1.33, 11.06)	0.013
3.42-3.39 (Glc, Tau)	2.46 (1.17, 5.14)	0.017
3.15-3.13 (Spermine, Histidine, Phenylalanine)	339.30 (2.44, $4.72x10^{4}$)	0.021
3.12-3.09 (polyamines)	$4.81x10^{3}$ (9.53, $2.43x10^{6}$)	0.008
2.38-2.37 (TBD)	$4.21x10^{4}$ (20, $8.87x10^{7}$)	0.006
2.36-2.31 (Glutamate)	2.58 (1.15, 5.78)	0.021
2.15-2.11 (Glu,Gln,GSH)	4.61 (1.67, 12.72)	0.003
1.91-1.89 (TBD)	59.05 (3.63, 961.34)	0.004
1.75-1.74 (TBD)	$2.87x10^{3}$ (5.33, $1.55x10^{6}$)	0.013
1.73-1.63 (TBD)	7.34 (1.92, 28.07)	0.004
1.6-1.57 (TBD)	0.03 ($1.74x10^{-3}$, 0.67)	0.026
1.49-1.46 (Ala)	6.66 (2.02, 21.97)	0.002
1.06-1.03 (Val)	14.29 (1.80, 113.58)	0.012
1.00-0.94 (Val, Lipids)	1.75 (1.09, 2.80)	0.02

Comparison of tissue adjacent to benign tumors (n=5, all oncocytoma) with tissue adjacent to the malignant tumors (n=13), screening did not reveal any FDR<0.05. When the tissue adjacent to benign tumors (n=5, all oncocytoma) were compared to benign tumors (n=17), (Table 6), there were 7 ROIs that differed in median relative intensities. Metabolites within these spectra include histidine, phenylalanine, phosphocholine, serine, spermine, and alanine, as well as some metabolites that are yet to be identified in the 3.57-3.56, 1.91-1.89, 1.75-1.74, and 1.73-1.63 ppm spectral regions. Comparison of AML to oncocytoma demonstrated that greater levels of histidine, phenylalanine, phosphocholine, serine, scylla-inositol, glycerophosphocholine, glutamate, glu,

gln, glutathione, alanine, valine, and lipids were found in oncocytoma specimens. There were also higher levels of metabolites in the 4.35-2.42, 3.8-3.78, 3.69-3.67, 3.57-3.56, 2.38-2.36, 1.93-1.92, and 1.35-1.33 ppm spectral regions in oncocytoma relative to AML (Table 7)

Table 6. Comparison of median relative intensities (IQR) of benign tumor vs. tissue adjacent to benign tumor

ROI (ppm)	Benign tumor (N=17)	Tissue adjacent to benign tumor (N=5)	Wilcoxon rank sum P-value	FDR P-value
3.99-3.96 (Histidine, Phenylalanine, Phosphocholine, Serine)	2.88 (2.71, 2.99)	0.79 (0.32, 2.02)	0.0069	0.038
3.57-3.56 (TBD)	2.80 (2.49, 3.23)	1.14 (0.16, 1.49)	0.0042	0.045
3.15-3.13 (Spermine, Histidine, Phenylalanine)	0.64 (0.62, 0.71)	0.13 (0.002, 0.21)	0.0009	0.000
1.91-1.89 (TBD)	0.62 (0.55, 0.67)	0.19 (0.0003, 0.36)	0.0033	0.017
1.75-1.74 (TBD)	0.42 (0.37, 0.47)	0.09 (0.06, 0.16)	0.0033	0.017
1.73-1.63(TBD)	1.63 (1.51, 1.80)	0.67 (0.41, 0.95)	0.0033	0.019
1.49-1.46 (Alanine)	3.17 (2.69, 3.80)	1.06 (0.46, 1.25)	0.0015	0.001

Table 7. Comparison of median relative intensities (IQR) of oncocytoma vs. AML

ROI (ppm)	Oncocytoma (N=10)	AML (N=7)	Wilcoxon rank sum P-value	FDR P-value
4.35-4.24 (TBD)	2.32 (1.33, 2.66)	0.47 (0.03, 0.98)	0.0147	0.022
3.99-3.96 (Histidine, Phenylalanine, Phosphocholine, Serine)	1.79 (0.79, 2.48)	0.32 (0.03, 0.49)	0.0063	0.006
3.8-3.78 (TBD)	3.18 (2.96, 3.69)	1.11 (0.02, 1.43)	0.0006	4.773×10^{-5}
3.69-3.67 (TBD)	2.72 (2.04, 3.36)	0.34 (0.04, 1.29)	0.0063	0.012
3.57-3.56 (TBD)	1.30 (1.14, 1.72)	0.04 (0.70, 0.02)	0.0047	0.004
3.36-3.34 (Scylla-Inositol)	0.68 (0.56, 1.11)	0.11 (0.01, 0.73)	0.0318	0.046
3.22-3.21 (Phosphocholine, Glycerophosphocholine, Histidine)	4.29 (2.40, 6.72)	0.03 (0.0004, 0.19)	0.0063	0.001
2.38-2.37 (TBD)	0.22 (0.16, 0.27)	0.04 (0.008, 0.14)	0.0034	0.007
2.36-2.31 (Glutamate)	1.82 (1.47, 1.90)	0.90 (0.04, 1.33)	0.0063	0.007
2.15-2.11 (Glu,Gln,glutathione)	1.64 (1.24, 2.20)	0.68 (0.002, 1.27)	0.0112	0.015
1.93-1.92 (TBD)	0.49 (0.42, 0.60)	0.12 (0.00002, 0.27)	0.0006	4.773×10^{-5}
1.49-1.46 (Alanine)	1.18 (1.06, 1.72)	0.37 (0.0002, 0.70)	0.0034	0.003
1.35-1.33 (TBD)	5.82 (2.45, 8.97)	15.13 (9.41, 26.56)	0.0047	0.007
1.06-1.03 (Valine)	0.37 (0.28, 0.67)	0.08 (0.00002, 0.23)	0.0034	0.006
1.00-0.94 (Valine, Lipids)	2.33 (1.47, 2.98)	0.96 (0.47, 1.37)	0.0063	0.007

In summary, these in depth *ex vivo* analyses showed that HRMAS MRS identified metabolites that may help differentiate fat-poor AML from ccRCC and RCC from adjacent benign parenchyma. Our initial analysis from this cohort was presented virtually at the Annual Meeting of the American Urologic Association in May 2020, where we were awarded Best Poster for our work. Our manuscript for these results has been written and is in final editing for submission. The confidential updated draft, which includes data presented above, has been attached to this report in the Appedices.

- **What opportunities for training and professional development has the project provided?**
  This project has provided multiple opportunities for training and professional development by increasing our understanding the challenges and nuances of performing *in vivo* metabolomic imaging of the kidney and renal masses, as well as investigating and discovering novel *in vivo* and *ex vivo* metabolomic profiles of benign and malignant renal masses.

- **How were the results disseminated to communities of interest?**
  We have communicated the results to the multidisciplinary members of our research group and as discussed above, have presented our data at the Annual Meeting of the American Urologic Association in May 2020. Our manuscript for these results has been written and is in final editing for submission.

- **What do you plan to do during the next reporting period to accomplish the goals?**
  Nothing to report

Impact:

- **What was the impact on the development of the principal discipline(s) of the project?**

Our optimization of protocols for *in vivo* MRS has allowed us to better utilize this method and measure the metabolomic profiles of renal tumor tissue non-invasively. This is novel work and will be published in a peer-reviewed journal. Our *ex vivo* MRS of benign and malignant renal tumor tissue, including AML and RCC is also novel work and will allow us to gain a better understanding the metabolomic profiling of these tumors in TSC and sporadic patients. This is also novel work and will be published in a peer-reviewed journal.

- **What was the impact on other disciplines?**
  The findings from this work will help gain insight into the active metabolic pathways in AML and RCC in TSC and sporadic patients. This may lead to improvements in *in vivo* imaging, but also potentially therapeutics targeting the metabolic pathway.

- **What was impact on technology transfer?**
  Nothing to report.

- **What was the impact on society beyond science and technology?**
  We are hopeful that the findings from this study will ultimately improve the clinical care of patients with TSC, who suffer from renal involvement, including AML and other tumors.

Changes/Problems:

- **Changes in approach and reasons for change**

  Given the slow rate of recruitment to the study, we utilized fresh frozen renal mass tissue from the MGH GU Oncology Frozen Tumor Bank for *ex vivo* MRS. As discussed above, this approach was successful in allowing us to increase our numbers in metabolomic analysis.

- **Actual or anticipated problems or delays and actions or plans to resolve them**
  We anticipated initial slow enrollment into the research study, which was resolved by consenting patients with sporadic lipid-poor renal masses and TSC patients with lipid-rich renal masses.

- **Changes that had a significant impact on expenditures**
  Nothing to report.

- **Significant changes in use or care of human subjects, vertebrate animals, biohazards, and/or select agents**
  Nothing to report.

Products:

- **Publications, conference papers, and presentations**
  Our *ex vivo* MRS metabolomic analysis of fresh frozen MGH GU Tumor Bank tissue was presented at the Annual Meeting of the American Urologic Association in May 2020, where we were awarded Best Poster for our work. Our manuscript for these results has been written and is in final editing for submission.

- **Website(s) or other Internet site(s)**
  Nothing to report.

- **Technologies or techniques**
  Nothing to report.

- **Inventions, patent applications, and/or licenses**
  Nothing to report.

- **Other Products**

  Imaging data and associated clinical databases; biospecimen collections

Participants & Other Collaborating Organizations:

- **What individuals have worked on the project?**

Name:	*Adam S. Feldman, MD, MPH*
Project Role:	*PI*
Researcher Identifier (e.g. ORCID ID):	
Nearest person month worked:	*3*
Contribution to Project:	*Dr. Feldman is responsible for the overall performance of this study. He consents patients in his clinic and then oversees the progress. He coordinates meetings with the various members of the project research team to discuss progress, data and troubleshoot difficulties.*
Funding Support:	

Name:	*Edouard Nicaise*
Project Role:	*Research Assistant*
Researcher Identifier (e.g. ORCID ID):	
Nearest person month worked:	*6*
Contribution to Project:	*Mr. Nicaise coordinates subject scheduling for MRI with in vivo MRS, records and maintains all data, coordinates the acquisition of all specimens and assists with laboratory preparation of specimens for ex vivo MRS and other analyses.*
Funding Support:	

Name:	*Andrew Gusev*
Project Role:	*Medical Student*
Researcher Identifier (e.g. ORCID ID):	
Nearest person month worked:	*6*
Contribution to Project:	*Mr. Gusev helped to coordinate subject scheduling for MRI with in vivo MRS, record and maintain data, coordinate the acquisition of specimens and assisted with laboratory preparation of specimens for ex vivo MRS and other analyses.*
Funding Support:	
Name:	*Eva Ratai, PhD*
Project Role:	*Co-Investigator*
Researcher Identifier (e.g. ORCID ID):	
Nearest person month worked:	1
Contribution to Project:	*Dr. Ratai has expertise in in vivo MRS and has worked on the development of our in vivo MRS protocol in the kidney and interpretation of MRS data*
Funding Support:	

Name:	*Mukesh Harisinghani, MD*
Project Role:	*Co-Investigator*

Researcher Identifier (e.g. ORCID ID):	
Nearest person month worked:	1
Contribution to Project:	*Dr. Harisinghani has expertise in diagnostic multiparametric MRI of the kidney. He has worked to interpret the clinical MRI images and will help to correlate our metabolomic data with standard multiparametric MRI imaging data.*
Funding Support:	

Name:	*Leo Cheng, PhD*
Project Role:	*Co-Investigator*
Researcher Identifier (e.g. ORCID ID):	
Nearest person month worked:	1
Contribution to Project:	*Dr. Cheng has expertise in ex vivo MRS and has worked on the development of our ex vivo MRS protocol for renal tissues and interpretation of MRS data*
Funding Support:	

Name:	*Chin-Lee Wu, MD, PhD*
Project Role:	*Co-Investigator*
Researcher Identifier (e.g. ORCID ID):	
Nearest person month worked:	1
Contribution to Project:	*Dr. Wu has expertise in genitourinary pathology, kidney cancer in TSC and angiomyolipoma. He reviews all pathology associated with this study.*

Funding Support:	

Name:	*Elizabeth Thiele, MD*
Project Role:	*Co-Investigator*
Researcher Identifier (e.g. ORCID ID):	
Nearest person month worked:	1
Contribution to Project:	*Dr. Thiele is the Director of the Herscot TSC Center here at MGH and is very involved in the referral of patients to Dr. Feldman for clinical care and also for consideration of this study.*
Funding Support:	

Name:	*Elizabeth Henske, MD*
Project Role:	*Co-Investigator*
Researcher Identifier (e.g. ORCID ID):	
Nearest person month worked:	1
Contribution to Project:	*Dr. Henske is a leader in the care of TSC patients and an active part of our local TSC community. She is very involved in the referral of patients to Dr. Feldman for clinical care and also for consideration of this study.*
Funding Support:	

Name:	*Othon Iliopoulos, MD*
Project Role:	*Co-Investigator*
Researcher Identifier (e.g. ORCID ID):	

Nearest person month worked:	1
Contribution to Project:	*Dr. Iliopoulos has expertise in the clinical and basic biology of RCC, and specifically has expertise in the metabolic pathways in RCC pathogenesis*
Funding Support:	

- **Has there been a change in the active other support of the PD/PI(s) or senior/key personnel since the last reporting period**

  Nothing to report.

- **What other organizations were involved as partners?**

  Nothing to report.

Special Reporting Requirements:

Nothing to report.

Appendix:

Characterization of the metabolomic profile of fat-poor angiomyolipoma and clear cell carcinoma by high resolution magic angle spinning (HRMAS) magnetic resonance spectroscopy (MRS)

Melissa J. Huynh[1, 4] MD, Andrew Gusev[1], Francesco Palmas[3] PhD, Lindsey Vandergrift[3], Chin-Lee Wu[2] MD, Shulin Wu MD[2], Leo Cheng[2,3] PhD, Adam S. Feldman[1,4] MD MPH

[1]Department of Urology, Massachusetts General Hospital, Boston, MA, USA

[2]Department of Pathology, Massachusetts General Hospital, Boston, MA, USA

[3]Department of Radiology, Massachusetts General Hospital, Boston, MA, USA

[4]Harvard Medical School, Boston, MA, USA

Abstract word count:

Manuscript word Count:

Corresponding Author:

Adam S. Feldman, MD, MPH

Massachusetts General Hospital

55 Fruit St.

Boston, MA 02114

afeldman@mgh.harvard.edu

ABSTRACT

Background: Renal cell carcinoma (RCC) is a metabolic disease, with the various subtypes exhibiting aberrations in different metabolic pathways. Metabolomics may offer greater sensitivity for revealing disease biology than evaluation of tissue morphology. In this study, we investigate the metabolomic profile of RCC using high resolution magic angle spinning (HRMAS) magnetic resonance spectroscopy (MRS).

Methods: Surgical tissue samples were utilized from our frozen tissue bank obtained from radical nephrectomy or partial nephrectomy. Specimens were fresh frozen and then stored at -80ºC until analysis. Tissue HRMAS-MRS was performed and a MatLab-based curve fitting program was used to process the spectra to produce relative intensities for each analyzed spectral region of interest. There were 59 spectral regions of interest, and comparisons of the metabolomic profiles of various RCC histologies and benign tumors (angiomyolipoma (AML) and oncocytoma) were performed. False discovery rates were used from the response screening to account for multiple testing. Regions of interest with FDR <0.05 were reported as potential predictors of RCC rather than benign tumor, and based on these results, the Wilcoxon rank sum test was used to compare the median MRS relative intensities for those metabolites that may differentiate between RCC and benign tumor. Logistic regression was employed to determine odds ratios for risk of malignancy based on the abundance of each metabolite.

Results: There were 38 RCC (16 clear cell, 11 papillary, 11 chromophobe), 10 oncocytomas, 7 AMLs & 13 adjacent normal tissue specimens (matched pairs). Candidate metabolites for predictors of malignancy rather than benign tumor based on FDR p-values include histidine, phenylalanine, phosphocholine, serine, phosphocreatine, creatine, glycerophosphocholine, valine, glycine, myo-inositol, scylla-inositol, taurine, glutamine, spermine, acetoacetate & lactate. There are additional metabolite predictors, which have yet to be identified. Higher levels of spermine, histidine & phenylalanine at 3.15-3.13 ppm were associated with a decreased risk of RCC (OR $4x10^{-5}$, 95% CI $7.42x10^{-8}$, 0.02), while 2.84-2.82 ppm increased the risk of malignant pathology (OR 7158.67, 95% CI 6.3, $8.3x10^{6}$), and the specific metabolites characterizing this region remain to be identified. Tumor stage did not appear to affect the metabolomics of malignant tumors, suggesting that metabolites are more dependent on histologic subtype.

Conclusions: HRMAS-MRS identified many metabolites that may predict RCC. We demonstrated that those in the 3.14-3.13 ppm ROI were present in lower levels in RCC, while higher levels of metabolites in the 2.84-2.82 ppm ROI substantially increased the risk of RCC. Further research in a larger population is required to validate these findings.

INTRODUCTION

Renal cell carcinoma (RCC) comprises approximately 85% of all kidney tumors[1] and has one of the highest mortality rates among urological cancers[2]. While there are radiographic features on cross-sectional imaging that may help to differentiate a malignant tumor from a benign one, there are still instances where imaging can present a diagnostic challenge. This can subsequently lead to biopsy or unnecessary surgical intervention. Up to 30% of small renal masses undergoing partial nephrectomy demonstrate benign histology upon pathologic examination, and this comes with a significant cost burden[3].

The field of metabolomics aims to define the specific metabolites associated with a tissue, cell, organ or organism under normal conditions, and these can be compared to the metabolites observed under abnormal conditions, such as a disease state[4]. The most common techniques used to identify and characterize these metabolites are nuclear magnetic resonance (NMR) spectroscopy and mass spectroscopy (MS), with the latter being more sensitive and specific[4]. However, the tissue preparation and separation techniques involved in MS can be time-consuming. Similarly, metabolites generally need to be extracted from tissues into liquid samples for NMR analysis[5]. On the other hand, high resolution magic angle spinning (HRMAS) magnetic resonance spectroscopy (MRS) offers the unique advantage of allowing metabolomic analysis of intact tissues[6], thereby presenting the opportunity for development of *in vivo* platforms with the ability to identify tumor histology based on metabolic profiles in order to avoid biopsies and unnecessary interventions and their associated complications.

In this study, we investigated the metabolomic profile of RCC and compared it to that of benign parenchymal tissue adjacent to the malignant tumors and benign tumors (angiomyolipoma and oncocytoma) using HRMAS-MRS.

METHODS

Patient population

This retrospective study was approved by our institutional research board. There were 38 patients with RCC and 17 patients with benign tumors. Demographic and clinical information were collected. All surgical specimens were reviewed by one pathologist (C-L.W.).

Tissue processing and spectroscopy

Surgical tissue samples were utilized from our frozen tissue bank obtained from radical nephrectomy or partial nephrectomy. Specimens were frozen and then stored at -80ºC for at least 24 hours until the time of analysis. Tissue HRMAS-MRS was performed on a Bruker AVANCE spectrometer operating at 600 MHz. Three different spectra were recorded at 4ºC: one without water suppression, one with water suppression and long *T2* filters, and one with water suppression and short *T2* filters.

Candidate metabolites and statistical analysis

A MatLab-based curve fitting program developed by our laboratory was used to process the spectra to produce relative intensities for each analyzed spectral region of interest. There were 59 spectral regions of interest, and comparisons of the metabolomic profiles were performed using JMP Pro 14 (*Cary, NC*). Comparisons were made between RCC and benign tissue adjacent to the malignant tumor, as well as between RCC and benign tumors. False discovery rates (FDR) were used from the response screening to account for multiple testing. Regions of interest (ROI) with FDR <0.05 were reported as potential predictors of RCC rather than benign tumor or benign tissue adjacent to malignant tumor. Based on these results, the Wilcoxon rank sum test was used to compare the median MRS relative intensities for those metabolites that may differentiate between RCC and either benign tumor or benign tissue adjacent to malignant tumor. Logistic regression was used to determine odds ratios for risk of malignancy based on the abundance of each metabolite.

RESULTS

Patient characteristics

Baseline characteristics are presented in **Table 1**. There were 38 RCC specimens (16 clear cell, 11 papillary, 11 chromophobe) and 13 of these had adjacent normal tissue specimens, therefore there were 13 matched pairs. For benign tumors, there were 10 oncocytomas and 7 AMLs, and there was adjacent normal tissue for 5 of these samples. The mean age for those with RCC was 55.3 ± 11.4, and those with benign tumors had a mean age of 59.2 ± 12.2 years. There was a preponderance of males in the RCC group (71%). The majority of malignant tumors were pT1 tumors (70.3%).

Predictors of RCC compared to tissue adjacent to malignant tumor

Comparisons of median MRS relative intensities for RCC (n=38) versus tissue adjacent to the malignant tumor (n=13) are presented in **Table 2**. Only statistically significant spectral regions based on FDR screening are reported. There were 60 ROIs tested, and 16 were found to be statistically significant. Those denoted as TBD (to be determined) are undergoing further study to definitively identify and associate specific metabolites to the corresponding spectral regions.

Table 3 summarizes the ROIs that were found to differ in median MRS relative intensity and the odds ratios for risk of malignancy based on relative abundance. Of particular note, there was a greater amount of serine and phosphocreatine (3.95-3.94 ppm) in RCC specimens, with an odds ratio of 29.24 [95% CI: 2.47, 345.94], p=0.007, as well as glutamine (2.45-2.42 ppm) (OR 121.56 [95% CI 2.17, 6825.42]). There are also a number of metabolites in other spectral regions that differed in quantity between RCC and the tissue adjacent to the malignant tumor, the exact identities of which have yet to be elucidated. The greatest odds ratio for risk of malignancy was observed for metabolites in the 2.84-2.82 spectral region (7161.72 [95% CI 6.30, 8.14×10^6], p=0.013).

Predictors of RCC compared to benign tumor

Comparisons of median MRS relative intensities for statistically significant spectral regions based on FDR screening for RCC (n=38) and benign tumor (n=17) are presented in **Table 4**. There were 25 ROIs found to be candidates for predictors of RCC, with FDR<0.05. **Table 5** summarizes the ROIs that were found to differ in median MRS relative intensity and the odds ratios for risk of malignancy based on relative abundance. ROIs associated with significantly elevated risk of malignancy include: 4.09-4.08 (OR 6.67×10^7, 95% CI 1.47, 3.01×10^{15}), 3.9-3.89 (creatine, glycerophosphocholine; OR 155.04, 95% CI 8.49, 2.83×10^3), 3.5-3.49 (OR 5.15×10^3, 95% CI 25.82, 1.03×10^6), 3.15-3.13 (spermine, histidine, phenylalanine; OR 339.30, 95% CI 2.44, 4.72×10^4), 3.12-3.09 (polyamines; OR 4.81×10^3, 95% CI 9.53, 2.43×10^6), 2.38-

2.37 (OR $4.21x10^4$, 95% CI 20, $8.87x10^7$), 1.91-1.89 (OR 59.05, 95% CI 3.63, 961.34), and 1.75-1.74 (OR $2.87x10^3$, 95% CI 5.33, $1.55x10^6$) ppm spectral regions.

Comparison of benign tumors

Comparison of tissue adjacent to benign tumors (*n*=5, all oncocytoma) with tissue adjacent to the malignant tumors (*n*=13), screening did not reveal any FDR<0.05. When the tissue adjacent to benign tumors (*n*=5, all oncocytoma) were compared to benign tumors (*n*=17), (**Supplementary Table 1**), there were 7 ROIs that differed in median relative intensities. Metabolites within these spectra include histidine, phenylalanine, phosphocholine, serine, spermine, and alanine, as well as some metabolites that are yet to be identified in the 3.57-3.56, 1.91-1.89, 1.75-1.74, and 1.73-1.63 ppm spectral regions. Comparison of AML to oncocytoma demonstrated that greater levels of histidine, phenylalanine, phosphocholine, serine, scylla-inositol, glycerophosphocholine, glutamate, glu, gln, glutathione, alanine, valine, and lipids were found in oncocytoma specimens. There were also higher levels of metabolites in the 4.35-2.42, 3.8-3.78, 3.69-3.67, 3.57-3.56, 2.38-2.36, 1.93-1.92, and 1.35-1.33 ppm spectral regions in oncocytoma relative to AML (**Supplementary Table 2**)

DISCUSSION

Up to 30% of small renal masses undergoing partial nephrectomy have been shown to harbor benign pathology with a cost burden of over $90 million between 2007 and 2014[3]. Proper identification of these benign tumors from RCC would avoid unnecessary surgical intervention and complications, as well as the costs associated with these procedures and outcomes.

The use of renal mass biopsy (RMB) may help to clarify pathology before proceeding to surgery. A systematic review and meta-analysis of 57 studies by Marconi *et al*. demonstrated that RMB has a 92% diagnostic rate. Percutaneous core biopsies have better test characteristics than fine-needle aspiration, with a sensitivity of 99.1% and 99.7%, and the median concordance rate between RMB and surgical pathology was 90.3%. However, the use of RMB is not without its own risks, including hematuria and hematomas. The median complication rate in the meta-analysis was 8.1%. While the majority are Clavien 1 complications, Claven 3a complications were also reported (embolization for pseudoaneurysm). As such, the use of metabolomics presents a platform by which patients may be able to avoid unnecessary intervention and complications, while distinguishing RCC and its histologically unique variants from benign renal masses.

Renal cell carcinoma is a highly metabolic disease, with aberrations in various enzymes in the tricarboxylic acid (TCA cycle). ccRCC is known to be characterized by increased glycolysis and reductive metabolism of glutamine and suppressed glucose oxidation via the TCA cycle[7,8,9]. Courtney *et al*. also provide evidence that metabolic profiles of ccRCC are consistent with the *Warburg effect* in human tumor, such as increased lactate from the shunting of pyruvate away from the TCA cycle[9]. Another study comparing fresh frozen matched ccRCC tumors and adjacent normal tissue pairs demonstrated that the levels of glucose, glucose-6-phosphate, and fructose-6-phosphate more than doubled in abundance in ccRCC[8]. Moreover, increased levels of intermediate metabolites such as 6-phosphogluconate suggested that ccRCC shunts metabolites towards the pentose phosphate pathway to produce ribose 5-phosphate and NADPH as sources of energy. It is also known that hypoxia-inducible factor (HIF), which is upregulated in renal cell carcinoma, causes increased glutamine utilization and accumulation of lactate and other glycolytic metabolites[7,9,10,11]. In our study, lactate and glutamine levels were found in higher levels in RCC samples compared to normal tissue adjacent to the tumor, and an increased glutamine level conferred over a 100-fold higher risk of harboring RCC.

Previous metabolomic and transcriptomic studies have shown that there are changes in lipid metabolism associated with the development of RCC[12]. There is an increase in the biosynthesis of lipids in many advanced ccRCC tumors, as well as HIF1α-mediated upregulation of lipid receptors and lipid storage genes, which may act to offset the tumors' compromised ability to obtain and utilize extracellular lipids. β-

oxidation of fatty acids has been reported to be upregulated in cancer cells as an alternative pathway for energy production[13]. Van der Mijn *et al*. demonstrated that changes in lipid metabolism are also seen in early stage ccRCC in the transgenic mouse model[12]. In our study, metabolites in the 1.00-0.94 ppm spectral region, which includes lipid metabolites, were found to be increased in RCC, and it was associated with a 1.75 times greater risk of finding RCC rather than a benign tumour (95% CI 1.09-2.80), consistent with some of the existing literature.

In terms of amino acid metabolism, Hakimi *et al*. described in their metabolomic study that amino acid biosynthesis and metabolism is decreased in ccRCC compared to the adjacent normal tissue, including phenyalanine, histidine, tyrosine, tryptophan, valine, leucine, isoleucine, taurine, glycine, serine and threonine. Our results also demonstrated decreased levels of metabolites in the 3.99-3.96 and 3.15-3.13 ppm regions, which potentially represent phenylalanine and histidine. Additionally, metabolites in regions representing glycine (3.55-3.52 ppm), taurine (3.24-3.23 ppm), tryptophan (4.07-4.05 ppm) were also decreased in RCC samples compared to adjacent normal tissue. The finding of decreased glycine was not reported in other studies, though it is used to synthesize glutathione (GSH), which has been found in elevated quantities in RCC in several studies[7,8,11]. Our results also corroborated this finding, with increased levels of metabolites in the 2.15-2.11 ppm region, which includes GSH. While valine was not found to differ significantly between RCC and the adjacent normal tissue in our study, valine was found in greater quantities in RCC compared to benign tumours.

Despite attempts at characterizations based on radiologic findings alone, there are still quite a number of patients who ultimately undergo surgery and are found to have benign findings on final pathology. NMR offers the ability to analyze intact tissue with reproducibility, therefore the ability to profile metabolites without subjecting the patient to the harms and complications of biopsy is an attractive possibility. However, MS combined with chromatography has the ability for higher throughput and with greater sensitivity, though it requires an extraction process to produce a sample for analysis[7]. The notion of biomarkers derived from serum or urine samples has been explored, but there have been inconsistent findings across various studies potentially secondary to differences in techniques in handling and processing the samples[14]. Thus, given the shortcomings of previous strategies and non-invasive biomarkers, there remains a need for techniques to accurately diagnose and characterize RCC without resorting to biopsies, and HRMAS MRS may have the potential to fulfill that need.

Another point of interest would be to determine whether or not there is any “halo effect” of metabolites from the tumors leaching into the adjacent benign parenchyma. Based on metabolite-tracing experiments, Sousa *et al.* have hypothesized that nutrients may be shuttled between tumor cells and normal tissue to promote proliferation of tumor cells in pancreatic ductal adenocarcinoma[15]. Reznik *et al.* considered that such a mechanism could also be present in ccRCC, but they note that correlations between tumor and normal tissue metabolite concentrations may vary based on the specific mechanism of shuttling present, such as passive vs. active transport of metabolites[16]. Identification of these compounds in future metabolite-tracing studies may help to provide more insight into these mechanisms.

There are several limitations to our study. Firstly, we are limited by the number of patients and pathologic specimens available. As a result of the limited number of samples, we pooled all RCC samples into a single group of malignant tumours for comparison to adjacent normal tissues and benign tumours. However, the pathophysiology of ccRCC from the loss of *VHL* may result in a different metabolomic profile compared to other RCC histologies that arise from aberrations in different genes. Further studies to analyze the metabolomic signature of each RCC histology would be beneficial, as they exhibit different behaviours and degrees of aggressiveness. For example, if one could confidently ascertain the presence of a small chromophobe RCC rather than a ccRCC, a less aggressive management approach may be considered. Moreover, there are still a number of regions of interest that have yet to be characterized or confirmed for accuracy, in terms of the exact metabolites that they represent. Nonetheless, HRMAS-MRS has the potential to be further developed as a possible means of non-invasive diagnosis of RCC, as well as in other tumours.

CONCLUSION

While breakthroughs in cancer metabolism have led to growth in genomic, transcriptomic, and metabolomic profiling of tumors, there remains a relative paucity of metabolomic data on RCC. The means of identifying and measuring specific metabolites has previously proven to be particularly challenging, with studies relying primarily on investigating individual metabolic pathways and exhibiting wide variability among *ex-vivo* and *in-vitro* assays. Our study using HR-MAS may provide insight for future metabolomics research allowing *in vivo* diagnosis of renal tumours, as well as other malignancies.

REFERENCES

1. Motzer RJ, Jonasch E, Agarwal N, Alva A. NCCN Guidelines Index Table of Contents Discussion. *Kidney Cancer*. Published online 2019:64.

2. Cairns P. Renal cell carcinoma. Srivastava S, Grizzle WE, eds. *Cancer Biomark*. 2011;9(1-6):461-473. doi:10.3233/CBM-2011-0176

3. Kim JH, Li S, Khandwala Y, Chung KJ, Park HK, Chung BI. Association of Prevalence of Benign Pathologic Findings After Partial Nephrectomy With Preoperative Imaging Patterns in the United States From 2007 to 2014. *JAMA Surg*. 2019;154(3):225. doi:10.1001/jamasurg.2018.4602

4. Klassen A, Faccio AT, Canuto GAB, et al. Metabolomics: Definitions and Significance in Systems Biology. In: Sussulini A, ed. *Metabolomics: From Fundamentals to Clinical Applications*. Vol 965. Advances in Experimental Medicine and Biology. Springer International Publishing; 2017:3-17. doi:10.1007/978-3-319-47656-8_1

5. Heude C, Nath J, Carrigan JB, Ludwig C. Nuclear Magnetic Resonance Strategies for Metabolic Analysis. In: Sussulini A, ed. *Metabolomics: From Fundamentals to Clinical Applications*. Vol 965. Advances in Experimental Medicine and Biology. Springer International Publishing; 2017:45-76. doi:10.1007/978-3-319-47656-8_3

6. Giskeødegård GF, Cao MD, Bathen TF. High-Resolution Magic-Angle-Spinning NMR Spectroscopy of Intact Tissue. In: Bjerrum JT, ed. *Metabonomics*. Vol 1277. Methods in Molecular Biology. Springer New York; 2015:37-50. doi:10.1007/978-1-4939-2377-9_4

7. DiNatale RG, Sanchez A, Hakimi AA, Reznik E. Metabolomics informs common patterns of molecular dysfunction across histologies of renal cell carcinoma. *Urol Oncol Semin Orig Investig*. Published online May 2019:S1078143919301619. doi:10.1016/j.urolonc.2019.04.028

8. Hakimi AA, Reznik E, Lee C-H, et al. An Integrated Metabolic Atlas of Clear Cell Renal Cell Carcinoma. *Cancer Cell*. 2016;29(1):104-116. doi:10.1016/j.ccell.2015.12.004

9. Courtney KD, Bezwada D, Mashimo T, et al. Isotope Tracing of Human Clear Cell Renal Cell Carcinomas Demonstrates Suppressed Glucose Oxidation In Vivo. *Cell Metab*. 2018;28(5):793-800.e2. doi:10.1016/j.cmet.2018.07.020

10. Hoerner CR, Chen VJ, Fan AC. The 'Achilles Heel' of Metabolism in Renal Cell Carcinoma: Glutaminase Inhibition as a Rational Treatment Strategy. *Kidney Cancer*. 2019;3(1):15-29. doi:10.3233/KCA-180043

11. Wettersten HI, Hakimi AA, Morin D, et al. Grade-Dependent Metabolic Reprogramming in Kidney Cancer Revealed by Combined Proteomics and Metabolomics Analysis. *Cancer Res*. 2015;75(12):2541-2552. doi:10.1158/0008-5472.CAN-14-1703

12. van der Mijn JC, Fu L, Khani F, et al. Combined Metabolomics and Genome-Wide Transcriptomics Analyses Show Multiple HIF1α-Induced Changes in Lipid Metabolism in Early Stage Clear Cell Renal Cell Carcinoma. *Transl Oncol*. 2020;13(2):177-185. doi:10.1016/j.tranon.2019.10.015

13. Ferreira LMR. Cancer metabolism: The Warburg effect today. *Exp Mol Pathol*. 2010;89(3):372-380. doi:10.1016/j.yexmp.2010.08.006

14. Rodrigues D, Monteiro M, Jerónimo C, et al. Renal cell carcinoma: a critical analysis of metabolomic biomarkers emerging from current model systems. *Transl Res*. 2017;180:1-11. doi:10.1016/j.trsl.2016.07.018

15. Sousa CM, Biancur DE, Wang X, et al. Pancreatic stellate cells support tumour metabolism through autophagic alanine secretion. *Nature*. 2016;536(7617):479-483. doi:10.1038/nature19084

16. Reznik E, Luna A, Aksoy BA, et al. A Landscape of Metabolic Variation across Tumor Types. *Cell Syst*. 2018;6(3):301-313.e3. doi:10.1016/j.cels.2017.12.014

Table 1. Baseline patient characteristics

	RCC (N=38)	**Benign tumors (N=17)**	**P-value**
Age (years) (mean ± SD)	55.3 ± 11.4	59.2 ± 12.2	0.2651
Sex (n, %)			0.012
Males	27 (71)	6 (35.3)	
Females	11 (29)	11 (64.7)	
Race (n, %)			0.260
White	97 (97.4)	16 (94.1)	
Black	0 (0)	0 (0)	
Hispanic	1 (2.6)	1 (5.9)	
Surgery			0.965
Radical nephrectomy	22 (59.5)	10 (58.8)	
Partial nephrectomy	15 (40.4)	7 (41.2)	
Missing	1 (2.6)	0 (0)	
Median tumor size (cm, IQR)	4.35 (3.2, 6.5)	4.9 (3.3, 8)	0.5496
Tumor Stage (n, %)			N/A
T1	26 (70.3)	-	
T2	2 (5.4)	-	
T3	9 (23.7)	-	
T4	0 (9)	-	
Missing	1 (2.6)	-	

Table 2. Comparison of median relative intensities (IQR) of RCC vs. tissue adjacent to malignant tumor

ROI (ppm)	RCC (N=38)	Tissue adjacent to malignant tumor (N=13)	Wilcoxon rank sum P-value	FDR P-value
4.07-4.05 (Myo-Inositol)	0.80 (0.50, 1.30)	1.85 (1.44, 2.24)	0.0025	0.026
4.02-4.00 (TBD)	1.21 (0.69, 2.06)	0.50 (0.22, 0.85)	0.0069	0.033
3.99-3.96 (Histidine, Phenylalanine, Phosphocholine, Serine)	1.26 (0.87, 1.89)	2.56 (1.46, 3.37)	0.0089	0.011
3.95-3.94 (Serine, Phosphocreatine)	0.77 (0.33, 1.19)	0.30 (0.002, 0.46)	0.0006	0.002
3.93-3.91 (Creatine, Glycerophosphocholine)	1.28 (0.91, 1.60)	0.69 (0.30, 1.31)	0.0069	0.011
3.61-3.59 (Myo-Inositol, Glycerophosphocholine,	0.96 (0.65, 1.20)	1.68 (1.49, 1.93)	0.0005	0.004
3.55-3.52 (Glycine)	1.92 (1.34, 3.10)	4.03 (2.90, 4.32)	0.0019	0.022
3.36-3.34 (Scylla-Inositol)	0.55 (0.35, 0.77)	1.34 (0.91, 1.53)	0.0019	0.004
3.24-3.23 (Myo-Inositol, Taurine)	5.86 (3.97, 9.42)	4.32 (2.61, 5.20)	0.0260	0.028
3.22-3.21 (Phosphocholine, Glycerophosphocholine, Histidine)	0.69 (0.24, 2.06)	4.23 (3.46, 5.42)	<0.001	1.570×10^{-4}
3.15-3.13 (Spermine, Histidine, Phenylalanine)	0.21 (0.11, 0.35)	0.83 (0.49, 0.99)	<0.001	1.025×10^{-4}
2.84-2.82 (TBD)	0.28 (0.18, 0.45)	0.18 (0.12, 0.22)	0.0020	4.792×10^{-4}
2.45-2.42 (Glutamine)	0.51 (0.31, 0.73)	0.32 (0.24, 0.38)	0.0095	0.008
2.15-2.11 (Glu,Gln,glutathione)	1.95 (1.47, 2.46)	1.45 (1.26, 1.91)	0.0360	0.016
1.93-1.92 (Acetoacetate)	0.31 (0.19, 0.67)	0.77 (0.58, 1.63)	0.0008	0.034
1.35-1.33 (Lactate)	8.73 (5.53, 13.2)	5.24 (3.08, 8.07)	0.0146	0.011

Table 3. Odds ratios for risk of malignancy for metabolites identified as potential predictors of malignancy based on FDR P-value (reference group: tissue adjacent to malignant tumor)

Region of interest (ppm)	Odds ratios (OR, 95% CI)	P-value for OR
4.07-4.05 (Myo-Inositol, G6P, Tryptophan)	0.38 (0.18, 0.82)	0.013
4.02-4.00 (TBD)	3.13 (1.10, 8.85)	0.032
3.99-3.96 (Histidine, Phenylalanine, Phosphocholine, Serine)	0.34 (0.16, 0.71)	0.004
3.95-3.94 (Serine, Phosphocreatine)	29.24 (2.47, 345.94)	0.007
3.93-3.91 (Creatine, Glycerophosphocholine)	8.17 (1.77, 37.78)	0.007
3.61-3.59 (Myo-Inositol, Glycerophosphocholine)	0.13 (0.03, 0.490)	0.003
3.55-3.52 (Glycine)	0.59 (0.39, 0.90)	0.014
3.36-3.34 (Scylla-Inositol)	0.08 (0.02, 0.42)	0.003
3.24-3.23 (Myo-Inositol, Taurine)	1.35 (1.04, 1.76)	0.027
3.22-3.21 (Phosphocholine, Glycerophosphocholine, Histidine)	0.41 (0.25, 0.67)	<0.001
3.15-3.13 (Spermine, Histidine, Phenylalanine)	3.72×10^{-5} (7.42×10^{-8}, 1.87×10^{-2})	0.001
2.84-2.82 (TBD)	7161.72 (6.30, 8.14×10^{6})	0.013
2.45-2.42 (Glutamine)	121.56 (2.17, 6825.42)	0.02
2.15-2.11 (Glu,Gln,GSH)	3.96 (1.18, 13.28)	0.026
1.93-1.92 (Acetoacetate)	0.38 (1.13, 1.09)	0.072
1.35-1.33 (Lactate)	1.22 (1.03, 1.45)	0.023

Table 4. Comparison of median relative intensities (IQR) of RCC vs. benign tumor

ROI (ppm)	RCC (N=38)	Benign tumor (N=17)	Wilcoxon rank sum P-value	FDR P-value
4.09-4.08 (TBD)	0.04 (0.0007, 0.1226)	0.0017 (0.0002, 0.0039)	0.0067	0.010
4.07-4.05 (Myo-Inositol, G6P, Tryptophan))	0.80 (0.50, 1.30)	1.78 (1.19, 2.65)	0.0097	0.016
4.02-4.00 (TBD)	1.21 (0.69, 2.06)	0.25 (0.13, 0.57)	0.0002	3.352×10^{-4}
3.9-3.89 (Cr, GPC)	0.90 (0.58, 1.13)	0.42 (0.10. 0.68)	<0.001	6.573×10^{-5}
3.86-3.85 (TBD)	0.81 (0.43, 1.14)	0.16 (0.008, 0.39)	<0.001	6.573×10^{-5}
3.84-3.81 (Glc)	1.30 (0.96, 1.70)	0.59 (0.03, 0.97)	0.0002	3.352×10^{-4}
3.61-3.59 (Myo-Inositol, Glycerophosphocholine,	0.96 (0.65, 1.29)	1.85 (1.58, 2.23)	0.0025	0.004
3.57-3.56 (Gly)	1.69 (1.29, 2.19)	1.14 (0.16, 1.49)	0.0040	0.020
3.55-3.52 (Glycine)	1.92 (1.34, 3.10)	3.62 (2.42, 6.12)	0.0197	0.020
3.5-3.49 (TBD)	0.31 (0.17, 0.59)	0.008 (0.0003, 0.12)	<0.001	6.573×10^{-5}
3.48-3.46 (TBD)	0.56 (0.33, 0.87)	0.05 (0.006, 0.35)	0.0028	0.011
3.45-3.43 (TBD)	1.20 (0.77, 2.32)	0.60 (0.32, 0.87)	0.0013	0.004
3.42-3.39 (Glc, Taurine)	1.37 (0.89, 2.81)	0.59 (0.25, 1.28)	0.0032	0.010
3.15-3.13 (Spermine, Histidine, Phenylalanine)	0.21 (0.11, 0.35)	0.13 (0.002, 0.21)	0.0133	0.040
3.12-3.09 (polyamines)	0.22 (0.13, 0.32)	0.08 (0.009, 0.16)	0.0015	0.020
2.38-2.37 (TBD)	0.26 (0.18, 0.35)	0.16 (0.08, 0.24)	0.003	0.008
2.36-2.31 (Glutamate)	1.91 (1.32, 2.76)	1.47 (0.12, 1.84)	0.0197	0.002
2.15-2.11 (Glu,Gln, glutathione)	1.95 (1.47, 2.46)	1.27 (0.68, 1.69)	0.002	0.020
1.91-1.89 (TBD)	0.46 (0.24, 0.66)	0.19 (0.0003, 0.26)	0.001	0.002
1.75-1.74 (TBD)	0.21 (0.14, 0.35)	0.09 (0.06, 0.16)	0.004	0.004
1.73-1.63 (TBD)	1.35 (0.84, 1.90)	0.67 (0.41, 0.95)	0.0011	0.008
1.6-1.57 (TBD)	0.08 (0.0005, 0.19)	0.19 (0.002, 0.49)	0.0197	0.002
1.49-1.46 (Alanine)	2.03 (2.84, 1.52)	1.06 (0.46, 1.25)	<0.001	0.010
1.06-1.03 (Valine)	0.61 (0.28, 0.89)	0.28 (0.11, 0.39)	0.007	6.573×10^{-5}
1.00-0.94 (Valine, Lipids)	2.75 (1.89, 4.19)	1.47 (0.96, 2.48)	0.0108	0.010

Table 5. Odds ratios for risk of malignancy for metabolites identified as potential predictors of malignancy based on FDR P-value (reference group: benign tumor)

Region of interest (ppm)	Odds ratios (OR, 95% CI)	P-value for OR
4.09-4.08 (TBD)	$6.67x10^{7}$ (1.47, $3.01x10^{15}$)	0.045
4.07-4.05 (Myo-Inositol, G6P, Tryptophan))	0.45 (0.25, 0.82)	0.009
4.02-4.00 (TBD)	7.61 (2.04, 28.35)	0.002
3.9-3.89 (Cr, GPC)	155.04 (8.49, $2.83x10^{3}$)	0.001
3.86-3.85 (TBD)	61.72 (5.75, 662)	0.001
3.84-3.81 (Glc)	10.5 (2.68, 41.22)	0.001
3.61-3.59 (Myo-Inositol, Glycerophosphocholine,	0.24 (0.09, 0.62)	0.003
3.57-3.56 (Gly)	2.98 (1.21, 7.35)	0.018
3.55-3.52 (Glycine)	0.68 (0.50, 0.92)	0.012
3.5-3.49 (TBD)	$5.15x10^{3}$ (25.82, $1.03x10^{6}$)	0.002
3.48-3.46 (TBD)	9.90 (1.51, 64.89)	0.017
3.45-3.43 (TBD)	3.84 (1.33, 11.06)	0.013
3.42-3.39 (Glc, Tau)	2.46 (1.17, 5.14)	0.017
3.15-3.13 (Spermine, Histidine, Phenylalanine)	339.30 (2.44, $4.72x10^{4}$)	0.021
3.12-3.09 (polyamines)	$4.81x10^{3}$ (9.53, $2.43x10^{6}$)	0.008
2.38-2.37 (TBD)	$4.21x10^{4}$ (20, $8.87x10^{7}$)	0.006
2.36-2.31 (Glutamate)	2.58 (1.15, 5.78)	0.021
2.15-2.11 (Glu,Gln,GSH)	4.61 (1.67, 12.72)	0.003
1.91-1.89 (TBD)	59.05 (3.63, 961.34)	0.004
1.75-1.74 (TBD)	$2.87x10^{3}$ (5.33, $1.55x10^{6}$)	0.013
1.73-1.63 (TBD)	7.34 (1.92, 28.07)	0.004
1.6-1.57 (TBD)	0.03 ($1.74x10^{-3}$, 0.67)	0.026
1.49-1.46 (Ala)	6.66 (2.02, 21.97)	0.002
1.06-1.03 (Val)	14.29 (1.80, 113.58)	0.012
1.00-0.94 (Val, Lipids)	1.75 (1.09, 2.80)	0.02

SUPPLEMENTARY TABLES

Supplementary Table 1. Comparison of median relative intensities (IQR) of benign tumor vs. tissue adjacent to benign tumor

ROI (ppm)	Benign tumor (N=17)	Tissue adjacent to benign tumor (N=5)	Wilcoxon rank sum P-value	FDR P-value
3.99-3.96 (Histidine, Phenylalanine, Phosphocholine, Serine)	2.88 (2.71, 2.99)	0.79 (0.32, 2.02)	0.0069	0.038
3.57-3.56 (TBD)	2.80 (2.49, 3.23)	1.14 (0.16, 1.49)	0.0042	0.045
3.15-3.13 (Spermine, Histidine, Phenylalanine)	0.64 (0.62, 0.71)	0.13 (0.002, 0.21)	0.0009	0.000
1.91-1.89 (TBD)	0.62 (0.55, 0.67)	0.19 (0.0003, 0.36)	0.0033	0.017
1.75-1.74 (TBD)	0.42 (0.37, 0.47)	0.09 (0.06, 0.16)	0.0033	0.017
1.73-1.63(TBD)	1.63 (1.51, 1.80)	0.67 (0.41, 0.95)	0.0033	0.019
1.49-1.46 (Alanine)	3.17 (2.69, 3.80)	1.06 (0.46, 1.25)	0.0015	0.001

Supplementary Table 2. Comparison of median relative intensities (IQR) of oncocytoma vs. AML

ROI (ppm)	Oncocytoma (N=10)	AML (N=7)	Wilcoxon rank sum P-value	FDR P-value
4.35-4.24 (TBD)	2.32 (1.33, 2.66)	0.47 (0.03, 0.98)	0.0147	0.022
3.99-3.96 (Histidine, Phenylalanine, Phosphocholine, Serine)	1.79 (0.79, 2.48)	0.32 (0.03, 0.49)	0.0063	0.006
3.8-3.78 (TBD)	3.18 (2.96, 3.69)	1.11 (0.02, 1.43)	0.0006	4.773×10^{-5}
3.69-3.67 (TBD)	2.72 (2.04, 3.36)	0.34 (0.04, 1.29)	0.0063	0.012
3.57-3.56 (TBD)	1.30 (1.14, 1.72)	0.04 (0.70, 0.02)	0.0047	0.004
3.36-3.34 (Scylla-Inositol)	0.68 (0.56, 1.11)	0.11 (0.01, 0.73)	0.0318	0.046
3.22-3.21 (Phosphocholine, Glycerophosphocholine, Histidine)	4.29 (2.40, 6.72)	0.03 (0.0004, 0.19)	0.0063	0.001
2.38-2.37 (TBD)	0.22 (0.16, 0.27)	0.04 (0.008, 0.14)	0.0034	0.007
2.36-2.31 (Glutamate)	1.82 (1.47, 1.90)	0.90 (0.04, 1.33)	0.0063	0.007
2.15-2.11 (Glu,Gln,glutathione)	1.64 (1.24, 2.20)	0.68 (0.002, 1.27)	0.0112	0.015
1.93-1.92 (TBD)	0.49 (0.42, 0.60)	0.12 (0.00002, 0.27)	0.0006	4.773×10^{-5}
1.49-1.46 (Alanine)	1.18 (1.06, 1.72)	0.37 (0.0002, 0.70)	0.0034	0.003
1.35-1.33 (TBD)	5.82 (2.45, 8.97)	15.13 (9.41, 26.56)	0.0047	0.007
1.06-1.03 (Valine)	0.37 (0.28, 0.67)	0.08 (0.00002, 0.23)	0.0034	0.006
1.00-0.94 (Valine, Lipids)	2.33 (1.47, 2.98)	0.96 (0.47, 1.37)	0.0063	0.007